Modelling of Carbon-Carbon Composite Ablation in Rocket Nozzles

G.L. Vignoles, Y. Aspa, Michel Quintard

Modelling of Carbon-Carbon Composite Ablation in Rocket Nozzles

G.L. Vignoles, Y. Aspa, M. Quintard

PII: S0266-3538(10)00131-4
DOI: 10.1016/j.compscitech.2010.04.002
Reference: CSTE 4678

To appear in: *Composites Science and Technology*

Received Date: 1 July 2009
Revised Date: 26 March 2010
Accepted Date: 2 April 2010

Please cite this article as: Vignoles, G.L., Aspa, Y., Quintard, M., Modelling of Carbon-Carbon Composite Ablation in Rocket Nozzles, *Composites Science and Technology* (2010), doi: 10.1016/j.compscitech.2010.04.002

Modelling of Carbon-Carbon Composite Ablation in Rocket Nozzles

G. L. Vignoles*[,a], Y. Aspa[a,b,c], M. Quintard[b,c]

[a] *University Bordeaux 1*
Laboratoire des Composites ThermoStructuraux (LCTS)
UMR 5801: CNRS-Safran-CEA-UB1
Domaine Universitaire de Bordeaux
3, Allée de La Boétie, 33600 Pessac, France
[b] *Université de Toulouse ; INPT, UPS ; IMFT (Institut de Mécanique des Fluides de Toulouse) ;*
1, allée Prof. Camille Soula, 31000 Toulouse, France
[c] *CNRS ; IMFT ;*
F-31400 Toulouse, France

Abstract

The modelling of ablation of Carbon/Carbon (C/C) composites utilized as rocket engine hot parts is addressed under the angle of the competition between bulk transport of reactants and heterogeneous mass transfer, associated to reactivity contrasts between constituent phases. A numerical solver based on a simple model and built on a VOF technique allows direct simulation at two scales. Its application to actual complex materials is performed; the results are consistent with experimental data and help understanding the origin of the material behaviour, either in terms of acquired surface morphology or in terms of effective recession rate.

Key words:
A. Ceramic-matrix composites (CMCs) – C/C composites
B. Environmental Degradation – Ablation
C. Multiscale modelling

*Corresponding author
Telephone: +33 (0) 5 56 84 47 00
Fax number: +33 (0) 5 56 84 12 25

Email address: vinhola@lcts.u-bordeaux1.fr (G. L. Vignoles)

1. Introduction

In the high-technology field of rocket solid propulsion, for example in the case of Ariane V boosters, thermal protection materials constituting the nozzle and divergent inner walls are submitted to very high temperatures – up to $3000\,K$. Under such heavy solicitations, few materials can remain in the solid state. Among them, Carbon/Carbon (C/C) composites have several relative advantages [1]: excellent ratio of mechanical properties versus density at high temperature, small thermal expansion, cost-effective processing of thick and large parts [2, 3].

In spite of these performances, the thermochemical constraints lead to a recessive degradation of the C/C composite surface by mass loss or *ablation*. The causes of this mass loss is mainly oxidation [4], while mechanical erosion may also play a role.

The ablation of the composite walls acts at a macroscopic scale and modifies the device geometry: the throat section increases. This may lead to a thrust loss compared to the nominal performances of the propulsion system. Moreover, as the thickness of the parts is reduced, the insulating function of the composite is damaged and may lead to a degradation of bonding parts. This macroscopic change in the geometry is linked to a modification of the microscopic structure of the composite characterized by an increase of the surface roughness. Indeed, the surface acquires a multiscale roughness which has been observed using SEM microscopy as illustrated in [5, 6]. It is also reported in [1] that this roughness development leads to an increase by a factor 1.7 of the convective heat flux received by the composite, which in turn has an impact on the recession velocity. These observations illustrate the fact that ablation is a multiscale and multiphysics process involving strong couplings between recession, surrounding flow, heat and mass transfer.

Many experimental characterizations of ablative materials have been reported [7, 8, 9, 10, 11, 12]; they usually consist in SEM observations of the ablated surfaces as well as of recession rate measurements (in mm/s or in $g/s/m^2$). Usual patterns of the rough surfaces are fiber denudation at the

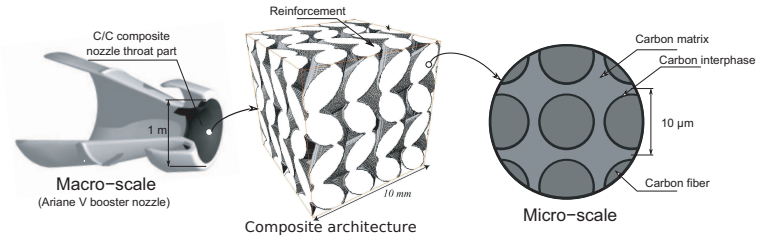

Figure 1: Multiscale structure of C/C composites used as nozzle throat parts.

micro-scale, due to a weak interphase or a weak matrix, and block denudation at macro-scale, mainly due to mechanical erosion of poorly bonded parts of the composite.

Numerous modelling studies have focused on the surrounding fluid behavior [4, 13, 14] with very simple descriptions of the composite properties. On the other hand, studies dealing with the structural and chemical complexity of such materials [15, 8, 16] do not take into account the transfer/recession coupling. The different points of view adopted in these works correspond to the fact that the composite heterogeneity and the global flow have different scales. The surrounding flow must be known at the part-scale, *i. e.*, a metric scale, whereas the composite is heterogeneous at a micrometer scale as illustrated by Figure 1. Therefore, the composite properties must be *up-scaled* in order to obtain an effective composite description suitable for macro-scale simulations.

In this paper, the focus is set on the competition between mass transfer and recession of the composite surface, with the objective of building an equivalent or effective macro-scale model yielding both a correct surface morphology and an adequate recession rate.

The document is organized as follows. In a first section, a description is given of the physico-chemical model that has to be modelled. Then, the model is set up, making use of some assumptions. A numerical method is outlined in a third part. Finally, its applications to two actual cases are described and discussed.

2. Description of the ablation conditions

2.1. Description of the ablative media

Carbon/carbon composites are part of the ceramic matrix composites (CMC). They are composed only of the element Carbon. Nevertheless, the material shows several scales of heterogeneity with a wide range of thermo-chemical properties [17].

The composite is formed by reinforcements and a matrix as illustrated in Figure 1. The reinforcement architecture can be textile-like (*i. e.*, stacked layers of fabric plies) or show a complex multidimensional and multiaxial geometry. The reinforcements are fiber bundles or yarns made of cylindrical carbon fibers of approximately $5\,\mu m$ radius. The reinforcements can be also composite materials when the fiber bundles are densified by a matrix as illustrated in the last picture of Figure 1. The matrix is deposited in the reinforcement architecture by liquid or vapor phase deposition [18]. In these two processes, the nanotexture and nanostructure of the obtained carbon will depend on the operative conditions as well as the chemical precursors (see *e.g.* [19] for gas-deposited pyrocarbons). The composite is treated at high temperature in order to reduce the density of micro-structural defects and to approach the graphite crystalline structure. Nevertheless, the obtained material shows significant spatial heterogeneity. The matrix has a lower coherence length of the ordered domains, which is known to be related to a higher reactivity [15, 20, 21, 17]. Two scales of heterogeneity are thus identified as illustrated in Figure 1: the micro-scale (fiber scale) with a characteristic length, l_μ, of a magnitude of ten microns and the mesoscale (reinforcement scale) with a characteristic length, l_m , of a magnitude of few millimeters. Therefore, the macro-scale effective property is the result of a double change of scale starting from the micro-scale. Assuming the separability of these heterogeneity scales, the composite will be described as an assembly of homogeneous but distinct phases. In addition to the different carbon phases, in some of the studied materials, especially the woven ones, there is a significant amount of macro-scale pores which will be taken into

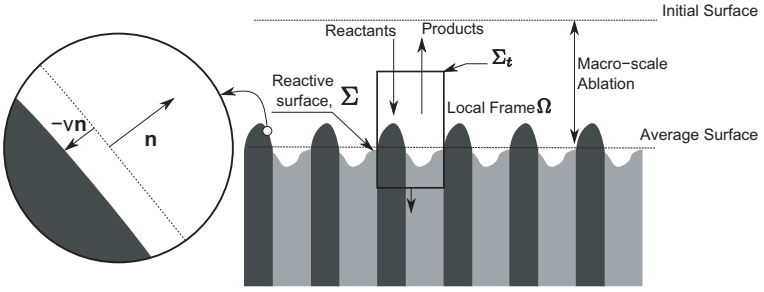

Figure 2: Microscale recession of the ablative surface.

account by an explicit description of the pore volume.

Since the curvature radius of the parts is large compared to the scales of interest in this work, it will be neglected in the developments. Due to the industrial process of part manufacturing, the composite surface will be assumed to be perfectly flat at the initial state.

2.2. Transfer phenomena

Under rocket firing conditions, the flow is highly turbulent in the core of the nozzle and the boundary layers themselves are turbulent. Computation of the mesoscale flow profile [22] shows that the longitudinal velocity is about $1000\,m.s^{-1}$ at $2\,mm$ of the ablative wall. The associated Reynolds number is then $Re_m = 5\,10^4$. At the micro-scale, the Reynolds number decreases and is about $Re_\mu = 250$. Modeling the turbulent momentum or mass transfer and its coupling with the surface recession is beyond the scope of this paper. In a preliminary attempt at understanding the concept of effective surface for ablative walls, we will only consider the laminar case, characteristic of the micro-scale. Moreover, compressibility of the fluid phase will be ignored.

During the ablation process, even though the macro-scale position of the ablative surface evolves due to recession, the thickness of the gasified material is small compared to the section of the nozzle throat (a few millimeters as compared to one meter), and is not significantly affected. The top of the boundary layer follows the macro-scale displacement of the ablative surface. Taking into account this evolution, the model is developed in a *local frame* which recedes with the surface as illustrated in figure 2.

The products of the propellant combustion contain numerous molecules

as described in [1]. Due to its very high temperature, the homogeneous reactions occurring in the gas phase are very fast and the gas mixture is always in a local chemical equilibrium [23]. Water being the most abundant among them, it will be the only modeled species. This molecule is sufficiently diluted in typical propergol combustion products [1] to be assumed to have no impact on the flow characteristics. Moreover, in the case of laminar boundary layers, the transverse pressure gradient is zero. On the other hand, there is a temperature gradient through the boundary layer, and, consequently, the equilibrium concentration of water is a function of the distance to the wall.

Mass transfer of water is governed by the chemical potential gradients for this species. In contrast with species which are not consumed or produced by the wall, there is a strong transverse gradient of the difference between the equilibrium chemical potential and its actual value. In response to this, there is a water diffusive flux oriented towards the wall, which has to be combined to a convective flux oriented tangentially. The magnitude of the convective flux decreases when getting close to the wall ; some distance away, it is so strong that it ensures completion of chemical equilibrium. In order to describe as simply as possible this transfer, we choose to display a model in which we substitute the chemical potential difference by the more familiar quantity concentration, which will be considered constant on the boundary layer limit.

2.3. Heterogeneous reactions

The composite surface is subjected to several heterogeneous reactions leading to the gasification of the solid wall. Numerous studies have been done in order to identify the chemical mechanisms and kinetics of carbon gasification at the composite scale under laboratory conditions [8, 24, 25, 26, 27, 16, 28, 29, 30]. Some studies were focused on the mass loss in nozzle throat applications [31, 1, 13, 14]. These studies agreed on the fact that mass loss in the nozzle throat application is mainly due to carbon oxidation by H_2O and CO_2 present in the gaseous products of propergols combustion

:

$$C(s) + H_2O(g) \rightarrow CO(g) + H_2(g)$$

$$C(s) + CO_2(g) \rightarrow 2CO(g)$$

Libby *et al.* [32] assume that the kinetic rates of the two oxidation mechanisms are identical. Under this assumption, water vapor being ten times more concentrated than carbon dioxide in the nozzle, the mass loss is mainly caused by H_2O.

The data from these studies can be collected into a global formalism with H_2O as a single oxidizing species, and an apparent first-order rate law with constant k :

$$k = K_s T_s e^{-E_a/RT_s} \tag{1}$$

In this expression, the values of the pre-exponential coefficient K_s lie between 1 and $50\, m.s^{-1}.K^{-1}$ and the activation energy E_a is about 40 $kcal.mol^{-1}$. The K_s variation is linked to the nanotexture and nanostructure of carbon and will depend on the considered solid phase.

3. Model set-up

The global ablation phenomenon is the result of the competition between several processes. In order to compare the influence of each of these processes, several dimensionless numbers have to be considered in addition to the previously defined Reynolds number :

- The mass Péclet number $Pe_\mu = \frac{u_0\, l_\mu}{D}$, where u_0 is the magnitude of the reference fluid velocity in the global frame, compares the velocity of advective to diffusive transfer mechanisms.

- The Damköhler number $Da_\mu = \frac{k\, l_\mu}{D}$ compares the surface reaction to the diffusion process. In the absence of advection, large values of Da lead to a diffusion-limited process for which the wall concentration is close to zero and the mass loss does not depend anymore on the reactivity k. On the contrary, when $Da \ll 1$, reaction is the limiting factor and

the concentration field tends to be uniform at the value imposed at the upper part of the boundary layer.

- The condensation ratio $\varpi = \frac{c_0}{c_s}$, which is the ratio between the recession and reaction velocity, is also the ratio between the solid volume concentration c_s and the gas concentration c_b in the bulk phase, close to the top of the boundary layer.

In the present application, the rate constant ranges between 10^{-1} and 200 $m.s^{-1}$, the diffusion coefficient is close to 10^{-4} $m^2.s^{-1}$, and, taking l_μ as a reference length, the dimensionless numbers take approximately the following values : $Pe = 500$, $Da \in [10^{-2}, 20]$, $\varpi = 3\,10^{-4}$. The proposed range for the Damköhler number is due to the range on the pre-exponential factor, K_s, defined in equation (1).

The obtained value of the Péclet number suggests that, even at the micro-scale, mass transfer is dominated by advection. However, in a recent study of the effective reaction rate for a rough surface, it has been shown [33] that the effective reaction rate is not sensitive upon the Péclet number below a value about Pe=500, for a wide range of Damköhler numbers. This indicates that a purely diffusive analysis has a relatively broad applicability range.

The condensation ratio shows that recession is slow compared to reaction. Moreover as $\frac{\varpi}{Da} \ll 1$, recession is slow compared to diffusion relaxation. The diffusion-reaction process is not influenced by the recessive displacement of the surface and velocity in the local frame can be identified with the velocity in the frame linked to a non recessive surface.

In a first approach, we will assume that the Péclet and the condensation numbers are small, i.e., we neglect advection effects, and the obtained model can be written :

$$\frac{\partial c}{\partial t} - D\Delta c = 0 \text{ in } \Omega \tag{2}$$

$$\mathbf{n}.(-D\nabla c) - k\,c = 0 \text{ on } \Sigma \tag{3}$$

$$\mathbf{v} + \frac{k\,c}{c_s}\mathbf{n} = 0 \text{ on } \Sigma \tag{4}$$

Equation 2 is a pure transient diffusion equation describing the reactant transport in the volume above the surface, equation 3 describes the matching of the incoming reactant flux and of the heterogeneous reaction rate at the surface (in which we have neglected the impact of the surface velocity), and equation 4 describes the surface recession with $\mathbf{v}$ being the surface velocity. This is comparable to the model conditions derived for the study of ablative thermal protection system C/C components [34]. However there will be a difference when applying this model to the large scale evolution of the materials, as shown later.

4. Numerical approach for the recession model

The problem for the recessive model requires the description of a moving interface. Interface tracking methods can be divided into two different general approaches. The first idea is to have a Lagrangian tracking of the interface. In this technique, the velocity of each node of the interface is computed and the geometry is rebuilt at each time step. Such a method can be used in a classical finite element procedure. Nevertheless, the geometry actualization and the associated re-meshing contribute to a high CPU time. The second method is a Eulerian description of the interface. In this method the problem which is written for each phase is transformed into a continuous formulation valid everywhere in the computed domain. In this class of method, different possibilities are available, such as the VOF (Volume of Fluid) method [35], level-set approaches [36], and many other phase-field approximations (see for instance the model of [37] for describing crystal growth).

4.1. Description of the method

This work makes use of a VOF method, featuring a Piecewise Linear Interface Calculation (PLIC) [38] because of its ability to work with non-differentiable surfaces. Indeed, the major difficulty for the problem under consideration lies in the description of the interface. The micro-scale observation of the ablated material [8, 24, 39, 5] shows that ablation leads to sharp edges.

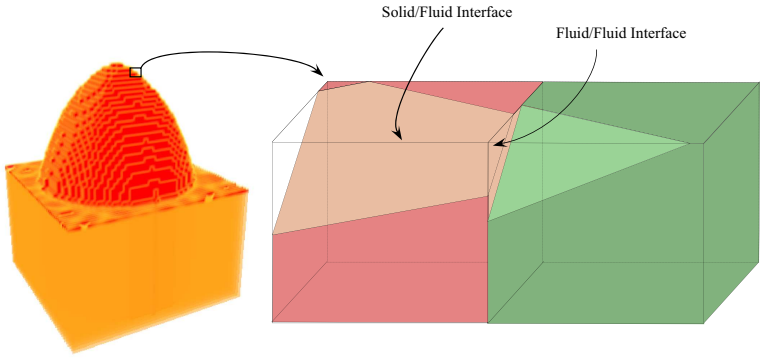

Figure 3: Interface description at the voxel scale.

In the PLIC description, the interface is modeled by local planar surfaces, whose positions and slopes are obtained from the phase indicator variable, as illustrated in Figure 3. We adapted this technique to our problem [40] with the idea to keep the possibility of sharp edges, as it is a characteristic feature of ablated surfaces. We do not describe here the details of the numerical technique, since it involves a fastidious listing of all possible geometrical situations.

The simulated domain is composed by a composite region topped by a fluid region. The composite region itself contains fluid voxels representing the pores and two types of solid voxels representing the different carbon phases (mainly the carbon fiber and matrix).

In problem (Eqs 2 - 4), the coupling between transfer equations and surface recession is not explicit. The mass transfer problem depends on the surface evolution through the geometry of Σ. Moreover, the displacement of the local frame in the global frame requires the knowledge of the average recession velocity. In order to produce a weak description of these couplings, the following loop is built:

1. Solve the concentration field in the local frame.
2. Evaluate the local recession velocities in the global frame.
3. Perform solid displacement in the local frame.

In order to have a complete form of the model, boundary conditions must be added to the previous balances. A Dirichlet condition $c = c_0$ is chosen at the

upper boundary and $c = 0$ at the bottom boundary. As the reactant does not diffuse in the solid phase, this condition has no impact on the simulations of dense composites. When the simulated composite is porous, the solid domain is chosen thick enough to produce a total consumption of the reactant before the bottom of the domain. Periodicity conditions are used along the vertical sides. The initial surface of the composite is chosen perfectly flat and the initial concentration field is zero: $c(\mathbf{x}, t = 0) = 0$. Because the recession time is large compared to diffusion time, the concentration field reaches a steady-state long before any significant first change is noticed in the wall position.

The diffusion-reaction problem is solved implicitly. Once the concentration field is obtained, the local recession velocities in the global frame are evaluated from eq.(4). The evolved surface is then given by the use of PLIC formulation. The obtained algorithm is implemented into a FORTRAN 90 code later referred to as DiAbl3D.

The program has been tested on an ideal computational cell described in [6]. An analytical expression has been derived for the roughness morphology [5, 6] ; it extends the results given in [24] to the case of diffusion/reaction competition. The numerical results match satisfactorily the predicted surface equations, as well as the numerical results obtained by another code [41]. Figure 4 shows a rather good agreement between a simulated fibre profile and the analytical shape for intermediate values of Da. When Da becomes very close to zero, the code is in perfect agreement with the predicted shape, which is a straight cone.

5. Roughness evolution of actual C/C composites

In this section, the surface evolution of two different classes of composites, *i. e.*, with two different kinds of reinforcement architectures, is studied.

5.1. "4D" Reinforced structures

The "$4D$" composite is reinforced by millimetric bundles of parallel fibers organized following the four inner diagonals of a cube, as explained in [42, 43]

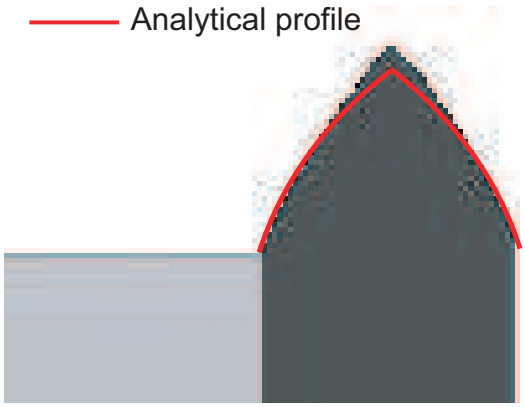

Figure 4: Steady ablation profile of a cylindrical fiber emerging from a matrix with $Da = 2$, $\phi_f = 0.5$, and $\tilde{K} = 4$.

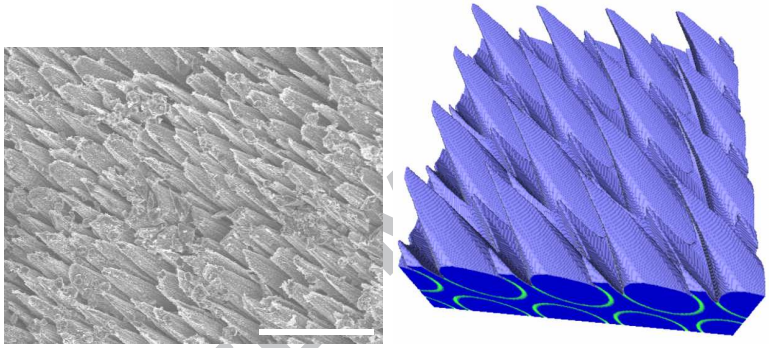

Figure 5: Left: SEM micrograph of the ablated surface of a bundle in 4D C/C composite. The bar length is approximately 30 μm. Right : simulation of the ablated bundle morphology.

and illustrated by the elementary pattern represented in figure 6, where the cylindrical reinforcements are shown in dark, and the inter-bundle matrix is shown in light. Their typical diameter size is millimetric. The bundles are themselves constituted by a dense packing of parallel fibers embedded in a carbon matrix.

Figure 5 (left) shows that, after ablation, the fibers and matrix emerge from the surface and have a characteristic shape with an approximate tip angle of 30°. The main cause of this morphology is the presence of a weak interphase between the fibers and the intra-bundle matrix (both having similar ablation resistances), associated to a low Da number [6].

In those conditions, it has been shown [6] that the effective reactivity of the bundle is close to the one of the weakest phase, that is, of the interphase.

This has been taken as a first clue to the identification of the individual reactivities af all phases, together with the assumption that the matrix has approximately the same reactivity as the fibers. The ratio between fiber and interphase reactivity has been varied systematically and the resulting steady-state angle tip was measured ; a correct match between experimental and modelled morphologies has been obtained for a ratio close to 8.5. Then, it has been confirmed that the effective reactivity of the bundle is very close to the reactivity of the weakest phase. It has also been checked that the transient time ($\approx$ 3 seconds) before development of the steady morphology is very short with respect to the total rocket firing time in usual tests.

Using these results, bundle-scale modelling is possible with our developed code by using the obtained effective reactivity. However, we know that turbulent effects at this scale might be important. To take into account these effects without having a strong modification of the mass transfer model, the diffusivity coefficient is artificially increased in order to represent the turbulent diffusivity. Values were matched to the turbulent kinematic viscosities obtained by a 1D boundary-layer code [22]. One missing input parameter is the reactivity ratio between the bundle and the inter-bundle matrix phases. Again, a simulation is run several times with a variation of the reactivity contrast, until the correct morphology is reproduced. The resulting evolution of the composite is represented in figure 6. One observes that, after a strong change in the composite surface, the roughness amplitude reaches a steady state. To obtain the very satisfactory agreement shown in Figure 7, the reactivity ratio between bundles and matrix is found to be 1/2. This means that the weakest phase at the macroscopic scale is twice as reactive as the strongest one.

An argument for this surprising agreement is the following. The total resistance to ablation is the result of several phenomena chained together in series : first, the heterogeneous reaction; second, the diffusion through the mass transfer boundary layer, which can be equated to the laminar bounday layer; third, mass transfer by convection and diffusion through the turbulent

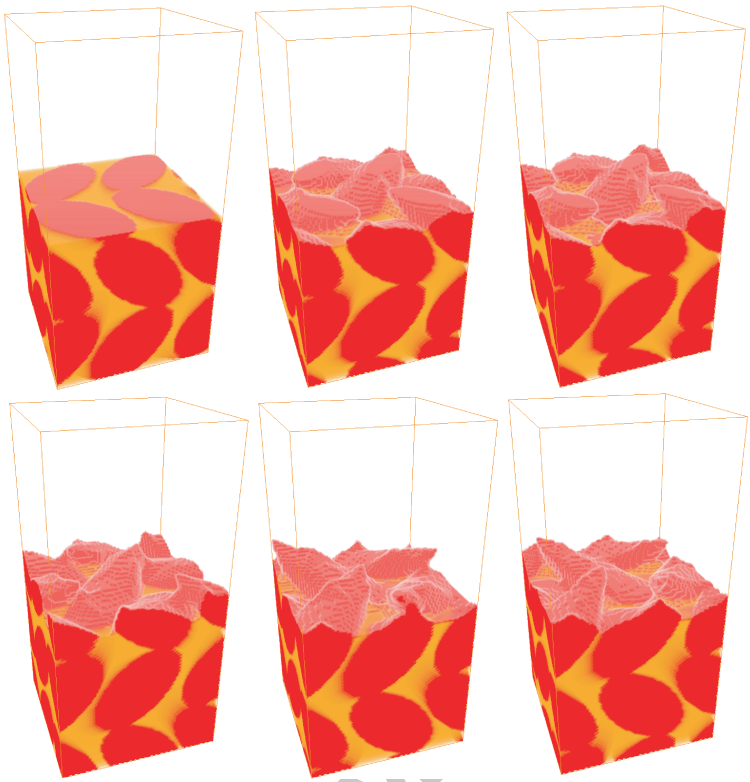

Figure 6: Evolution of the composite at millimeter scale for the 4D structure with $l_m = 5\,mm$ for time steps $t = 0, 0.25, 0.75, 1.25, 1.75, 2.25\,s$.

fluid. The most important resistances control the ablation rate as a whole. It appears that the transfer resistance in the turbulent fluid is not important. The controlling phenomena are then the heterogeneous reaction and the transfer through the laminar boundary layer. For the latter, the only critical parameter is the boundary layer thickness, that can be extracted from specific computations [22]. So, reducing the model to heterogeneous reaction and pure diffusion through a laminar boundary layer still allows to capture the main features of the wall recession dynamics.

5.2. Composites with woven architecture

Another class of C/C composites is prepared from preforms made of woven carbon fiber fabrics [44]. The matrix is infiltrated between the fibers by Chemical Vapor Infiltration, *i. e.*, a gas-phase route [45]. During this process, the tortuosity of the preform plays an important role by limiting the deposition in the composite core [46]. As a consequence, the composite

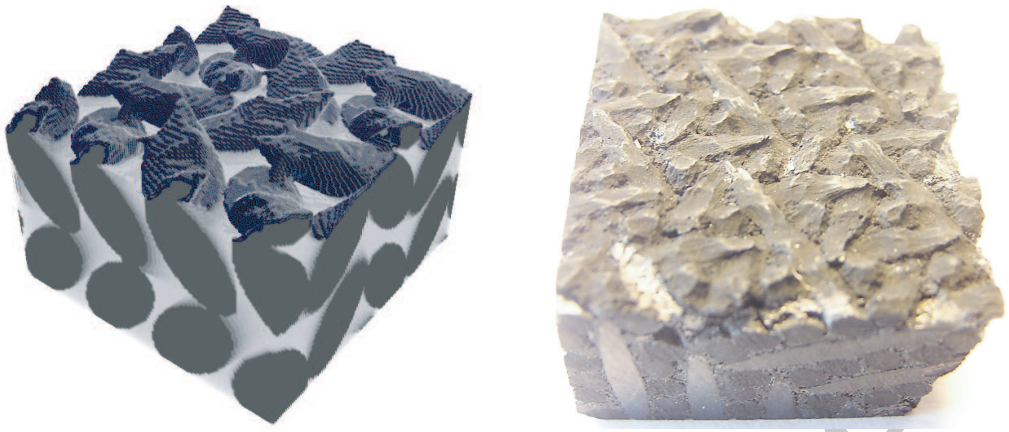

Figure 7: Comparison between simulated (left) and experimental (right) structures.

material at the end of the process still contains about 10% pore volume. In this section, DiAbl3D is used to investigate the role of the tortuosity of two different composites on their effective ablative behavior. Since the developed model cannot describe precisely the turbulent transfer occurring in the nozzle, the ablation process modeled here refers more to a purely diffusive oxidation of the material, *e.g.* in a laboratory furnace, than to the nozzle application. This study has been made for different Damköhler numbers. For a given composite, this dimensionless number is a function of temperature because of the exponential variation of the reactivity (Arrhenius law). The Damköhler values used in the simulation are therefore linked to the temperature of the experimental furnace.

Two different woven architectures were compared (they will be referred to as A and B). As the description of such architectures by analytic means is complex and poorly realistic, the structure of the native composite was obtained using X-ray tomography with a voxel dimension of $20 \times 20 \times 20 \mu m^3$. The scans allow to recognize three phases: the yarns, the surrounding matrix and the pores. A region of $2 \times 2 \times 6\, mm$ was extracted from the whole scanned region. Such a volume contains a representative number of yarns. The initial structure of composite A is illustrated in the first picture of figure 8.

The porosity was determined from the scans to be $\varepsilon_A = 10.4\%$ and $\varepsilon_B = 9.7\%$. The final tortuosity for molecular diffusion in the vertical di-

rection was determined from the scans as follows. A steady-state concentration field was computed using DiAbl3D by imposing an average vertical concentration gradient to the composite sample. This allows to calculate the effective diffusivity D_{eff} and, subsequently, the tortuosity, η_A and η_B. We found $\eta_A = \varepsilon_A \frac{D_{\text{eff}}}{D} = 15$ and $\eta_B = 26$. The obtained values show a good agreement with the values proposed by [47, 48] for fibrous materials having a 3D structure. The ablative evolution of composite A is shown in figure 8. As the composite has no stationary or even strictly periodic structure in the vertical direction the system does not reach a true steady-state profile. Nonetheless, the simulations have shown that after $0.2\,mm$ of recession, the thickness of the ablative front reaches a pseudo-steady state. At the studied temperatures, $T = 1850, 2300, 3000\,K$, the associated Damköhler number defined with yarn properties takes the values $Da = \frac{k_{\text{yarn}} l_m}{D} = 0.7,\ 1.1,\ 7$. Under such conditions, the reactant is totally consumed in the first millimeters of the composite and does not penetrate deep inside the porous structure.

Figure 8 shows that, at the lowest temperature ($T = 1850\,K$), the surface develops an important roughness. An estimation of the reaction front thickness was obtained using the maximum depth at which $c = 10^{-3} c_0$. The obtained values at this temperature are 1.1 mm for composite A and only 0.7 mm for composite B. So, gasification in composite B is limited to a thinner region than in the case of composite A. The obtained receding velocities are in the following ratio : $\frac{v_a|_A}{v_a|_B}(T = 1850\,K) = 1.24$. Under the chosen conditions, the ablation process occurs in a significant thickness of the porous material and is therefore influenced by the geometrical structure of the porous domain. The explanation for the difference in behavior between sample A and sample B is that the penetration of the reactant is facilitated in the less tortuous material (sample A), which leads to a larger global reaction rate. When temperature increases, *i. e.*, when Da increases, reaction occurs in a thinner domain. For instance, at $T = 3000\,K$, which represents the temperature of the nozzle throat, the wall remains flat and the reaction front thickness is less than $60\,\mu m$ for both composites. The difference of behavior

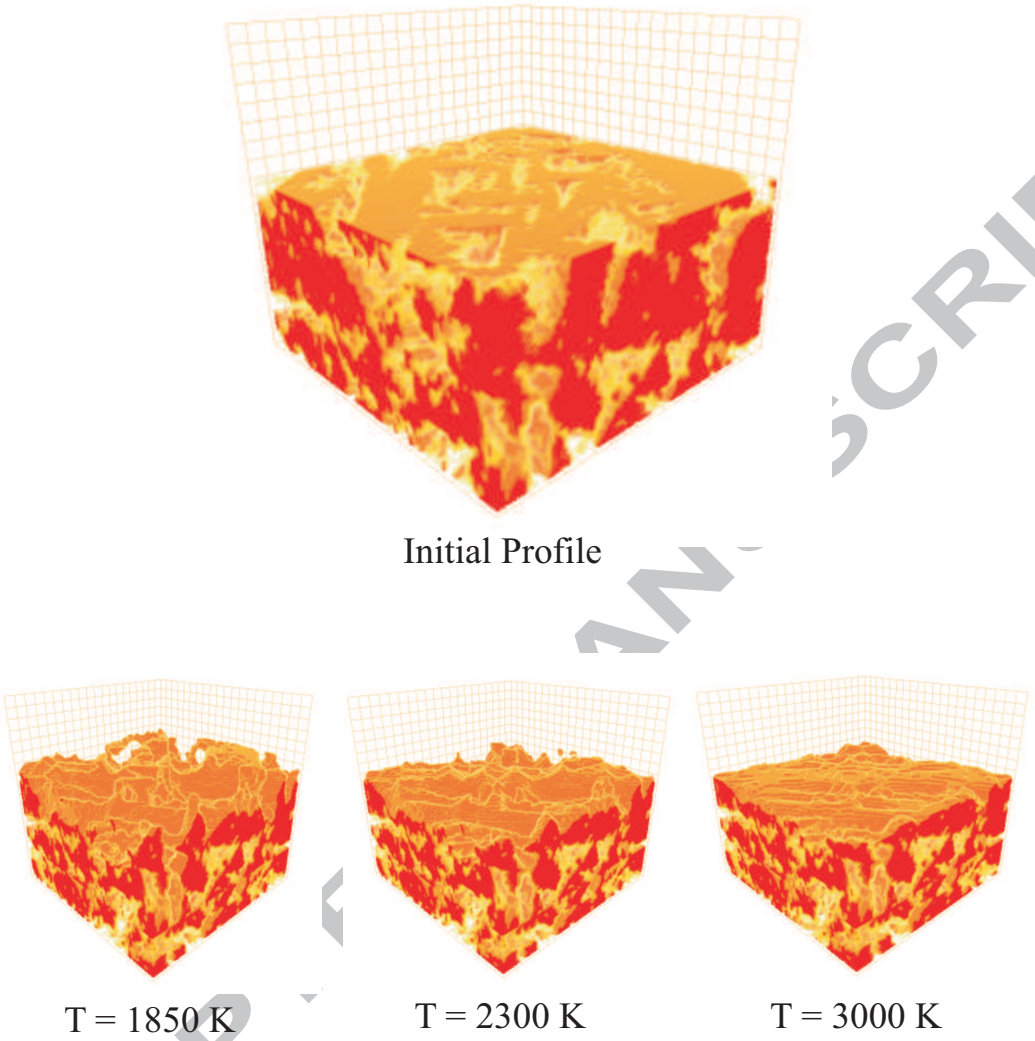

Figure 8: 3D initial and ablated morphologies obtained on a woven composite after $0.5mm$ of recession, for three different temperatures (*i. e.* Damköhler numbers).

between the two samples becomes negligible, as illustrated by the ablation velocity ratio value $\frac{v_a|_A}{v_a|_B}(T = 3000\,K) = 1.02$.

This study shows that at high temperature ($T > 2000\,K$), the composite architecture plays a less significant role on its ablation behavior. When temperature reaches such values, ablation occurs only at the surface of the porous wall, even at the mesoscale.

In conclusion, the numerical simulations have shown the importance of the Damköhler number on the obtained morphologies. All other parameters

remaining unchanged, a slower reaction rate leads to a higher roughness and an increase of the associated exposed surface.

6. Conclusion

This work has presented a modelling analysis of the surface evolution of C/C composites under ablation in rocket nozzle conditions. Previous studies had shown that the morphological parameters are directly linked to the material structure (reactivity contrast between constituents) and to the physico-chemical regime – chiefly the reaction/diffusion ratio translated by the Da number.

The ablative behavior of a complex two-scale architecture has been successfully performed, thanks to an inverse approach for the determination of the reactivity contrasts between phases.

The extension of the direct simulation to complex woven architectures confirm the impact of the Damköhler number on the recessive evolution that had been determined on ideal architectures. In the case of a reactive porous interface, the numerical simulations show that, when the heterogeneous reaction becomes faster (*i. e.*, for large values of Da), the reaction front becomes thinner and the global recession depends less on the pore space structure.

Another conclusion is that the effective recession rate for the composite is not given by a simple rule of mixtures – rather, in many conditions, a weakest-link rule applies. Reconstituting the morphology helps in identifying the weakest phase properties, even though they are not available as separate components.

These encouraging results have been obtained in spite of very crude approximations on the description of the gas flow surrounding the material. This very fact suggests that the material architecture is the primary element that determines its morphology after ablation, though the flow has an importance in some cases.

These results are of importance for the rocket nozzle designer, since the roughness and effective mass transfer coefficients may be assessed directly.

Entering these quantities in a rocket nozzle CFD code allows a better prediction of the final protection thicknesses and throat radius.

Depending on the application, it could be necessary to extend the presented work by taking into account stronger couplings with other transport mechanisms, in particular heat transfer, under the form of convection, conduction and radiation. Also, mass convection is a phenomenon that has been neglected in this first approach, and further work is ongoing to remove this rather strong hypothesis.

Acknowledgments

The authors wish to acknowledge Snecma Propulsion Solide (Safran group) for the industrial partnership and the French Defense Ministry for a PhD grant to Y.A.. J. Lachaud (LCTS, CEA) is acknowledged for helpful discussions.

References

[1] V. Borie, J. Brulard, G. Lengellé, An aerothermochemical analysis of carbon-carbon nozzle regression in solid-propellant rocket motors, in: 24th Joint Propulsion conference, AIAA/ASME/SAE/ASEE, Boston, MA, 1988.

[2] E. Savage, Carbon/Carbon composites, Chapman & Hall, London, 1993.

[3] L. M. Manocha, E. Fitzer, Carbon reinforcements and C/C composites, Springer, Berlin, 1998.

[4] K. Kuo, S. Keswani, A comprehensive theoretical model for carbon-carbon composite nozzle recession, Combustion Science and Technology 42 (1986) 177–192.

[5] G. Vignoles, Y. Aspa, J. Lachaud, Roughness evolution in ablation of carbon-based materials: multi-scale modelling and material analysis, in: K. Fletcher (Ed.), 5th European Workshop on Thermal Protection Systems and Hot Structures, Vol. SP-631 of ESA Confs. Procs., ESA-ESTEC, ESA, Noordwijk,The Netherlands, 2006.

[6] J. Lachaud, Y. Aspa, G. L. Vignoles, Physico-chemical ablation of carbon-carbon composites: Multi-scale analytical modeling in steady state, Int. J. of Heat and Mass Transfer 51 (2008) 2614–2627.

[7] E. Gulbransen, K. Andrew, F. Brassart, Ablation of graphite in oxygen and air at 1000-1400°c under flow conditions, Carbon 1 (4) (1964) 413 – 424.

[8] J. C. Han, X. D. He, S. Y. Du, Oxidation and ablation of 3D carbon-carbon composite at up to 3000°C, Carbon 33 (4) (1995) 473–478.

[9] Q. Tong, J. Shi, Y. Song, Q. Guo, L. Liu, Resistance to ablation of pitch-derived ZrC/C composites, Carbon 42 (12-13) (2004) 2495 – 2500.

[10] N. S. Jacobson, D. M. Curry, Oxidation microstructure studies of reinforced carbon/carbon, Carbon 44 (7) (2006) 1142–1150.

[11] J. Yin, X. Xiong, H. Zhang, B. Huang, Microstructure and ablation performances of dual-matrix carbon/carbon composites, Carbon 44 (9) (2006) 1690 – 1694.

[12] B. Chen, L.-T. Zhang, L.-F. Cheng, X.-G. Luan, Erosion resistance of needled carbon/carbon composites exposed to solid rocket motor plumes, Carbon 47 (6) (2009) 1474 – 1479.

[13] H. K. Chelliah, A. Makino, I. Kato, N. Araki, C. K. Law, Modeling of graphite oxidation in a stagnation-point flow field using detailed homogeneous and semiglobal heterogeneous mechanisms with comparisons to experiments, Combustion and Flame 104 (4) (1996) 469–480.

[14] F. S. Milos, Y. K. Chen, Comprehensive model for multicomponent ablation thermochemistry, in: 35th Aerospace Sciences Meeting & Exhibit, AIAA, Reno, NV, 1997.

[15] J. Rodríguez-Mirasol, P. A. Thrower, L. R. Radovic, On the oxidation resistance of carbon-carbon composites: Importance of fiber structure for composite reactivity, Carbon 33 (4) (1995) 545–554.

[16] R. Luo, J. Cheng, T. Wang, Oxidation behaviour and protection of carbon/carbon composites prepared using rapid directional diffused CVI techniques, Carbon 40 (2002) 1965–1972.

[17] J. Lachaud, N. Bertrand, G. L. Vignoles, G. Bourget, F. Rebillat, P. Weisbecker, A theoretical/experimental approach to the intrinsic oxidation reactivities of C/C composites and of their components, Carbon 45 (2007) 2768–2776.

[18] M. Lacoste, A. Lacombe, P. Joyez, R. A. Ellis, J. C. Lee, F. M. Payne, Carbon/carbon extendible nozzles, Acta Astronautica 50 (6) (2002) 357–367.

[19] G. L. Vignoles, F. Langlais, C. Descamps, A. Mouchon, H. L. Poche, N. Bertrand, N. Reuge, CVD and CVI of pyrocarbon from various precursors, Surf. Coat. Technol. 188-189 (2004) 241–249.

[20] F. A. Quli, P. A. Thrower, L. R. Radovic, Effects of the substrate on deposit structure and reactivity in the chemical vapor deposition of carbon, Carbon 36 (11) (1998) 1623–1632.

[21] S. Labruquère, X. Bourrat, R. Pailler, R. Naslain, Structure and oxidation of C/C composites: role of the interface, Carbon 39 (2001) 971–984.

[22] B. Aupoix, Couches limites bi-dimensionnelles compressibles. descriptif et mode d'emploi du code CLIC2, Rapport final RF1/5620.02-1/5620.05, ONERA, DMAE (Jan 1999).

[23] V. Borie, Y. Maisonneuve, D. Lambert, G. Lengellé, Ablation des matériaux de tuyères de propulseurs à propergol solide, Technical report 13, ONERA, Châtillon, France (Nov 1990).

[24] W. H. Glime, J. D. Cawley, Oxidation of carbon fibers and films in ceramic matrix composites: a weak link process, Carbon 33 (8) (1995) 1053–1060.

[25] W.-Y. Chen, A. Kulkarn, J. L. Milum, Stochastic modeling of carbon oxidation, AIChE 45 (1999) 2557–2570.

[26] N. S. Jacobson, T. A. Leonhardt, D. M. Curry, R. A. Rapp, Oxidative attack of carbon/carbon substrates through coating pinholes, Carbon 37 (1999) 411–419.

[27] L. Jiqiao, H. Baiyun, S. Gang, C. Tengfei, X. Xiang, Influence of porosity and total surface area on the oxidation resistance of C/C composites, Carbon 40 (2002) 2483–2488.

[28] C. A. A. Cairo, M. Florian, M. L. A. Graca, J. C. Bressiani, Kinetic study by TGA of the effect of oxidation inhibitors for carbon-carbon composite, Materials Science and Engineering A 358 (1-2) (2003) 298–303.

[29] C. Vix-Guterl, G. Bekri, J. Dentzer, S. Manocha, L. Manocha, P. Ehrburger, Reactivity in wet air of carbon/carbon composites with treated pitches, J. Anal. Appl. Pyrolysis 67 (2003) 341–357.

[30] P. Gao, H. Wang, Z. Jin, Study of oxidation properties and decomposition kinetics of three-dimensional (3-D) braided carbon fiber, Thermochimica Acta 414 (2004) 59–63.

[31] E. S. Golovina, The gasification of carbon by carbon dioxide at high temperatures and pressures, Carbon 18 (1980) 197–201.

[32] P. A. Libby, T. R. Blake, Burning carbon particles in the presence of water vapor, Combustion and Flame 41 (1981) 123–147.

[33] S. Veran, Y. Aspa, M. Quintard, Effective boundary conditions for rough reactive walls in laminar boundary layers, International Journal of Heat and Mass Transfer 52 (2009) 3712–3725.

[34] J. Lachaud, G. L. Vignoles, J.-M. Goyhénèche, J.-F. Epherre, Ablation of carbon-based materials : Multiscale roughness modelling, Composites Science and Technology 44 (2009) 1034–1041.

[35] S. W. J. Welch, J. Wilson, A volume of fluid based method for fluid flows with phase change, Journal of Computational Physics 160 (2000) 662–682.

[36] D. Adalsteinsson, J. Sethian, Transport and diffusion of material quantities on propagating interfaces via level set methods, Journal of Computational Physics 185 (2003) 271–288.

[37] C. Beckermann, H.-J. Diepers, I. Steinbach, A. Karma, X. Tong, Modeling melt convection in phase-field simulations of solidification, Journal of Computational Physics 154 (1999) 468–496.

[38] R. Scardovelli, S. Zaleski, Analytical relations connecting linear interfaces and volume fractions in rectangular grids, Journal of Computational Physics 164 (2000) 228–237.

[39] J. Lachaud, G. L. Vignoles, J. M. Goyhénèche, J. F. Epherre, Ablation in C/C composites: microscopic observations and 3D numerical simulation of surface roughness evolution, Ceramic Transactions 191 (2006) 149–160.

[40] Y. Aspa, J. Lachaud, G. Vignoles, M. Quintard, Simulation of C/C composites ablation using a VOF method with moving reactive interface, in: 12th European Conference on Composite Materials, ECS/AMAC, Biarritz, FRANCE, 2006.

[41] J. Lachaud, G. L. Vignoles, A brownian motion simulation technique to simulate gasification and its application to ablation, Computational Materials Science 44 (2009) 1034–1041.

[42] X. Aubard, C. Cluzel, L. Guitard, P. Ladeveze, Modelling of the mechanical behaviour of 4D carbon/carbon composite materials, Composites Science and Technology 58 (5) (1998) 701–708.

[43] X. Aubard, C. Cluzel, L. Guitard, P. Ladeveze, Damage modeling at two scales for 4D carbon/carbon composites, Computers & Structures 78 (1-3) (2000) 83–91.

[44] O. Coindreau, G. L. Vignoles, Assessment of geometrical and transport properties of a fibrous C/C composite preform as digitized by X-ray computed micro-tomography. Part I : Image acquisition and geometrical properties, J. Mater. Res. 20 (2005) 2328–2339.

[45] G. L. Vignoles, Modelling of CVI processes, Adv. Sci. Technol. 50 (2006) 97–106.

[46] I. Golecki, C. Morris, D. Narasimhan, US Patent no. 5 348 774 (1994).

[47] M. Tomadakis, S. Sortichos, Effect of fiber orientation and overlapping on Knudsen, transition and ordinay regime diffusion in fibrous substrates, in: Chemical Vapor Deposition of refractory metals and ceramics, Vol. 250 of Materials Research Society symposium proceedings, MRS, 1991.

[48] G. L. Vignoles, O. Coindreau, A. Ahmadi, D. Bernard, Assessment of geometrical and transport properties of a fibrous C/C composite preform as digitized by X-ray computed micro-tomography. Part II : Heat and gas transport, J. Mater. Res. 22 (6) (2007) 1537–1550.

Nomenclature

Greek symbols

η	Tortuosity in the vertical direction.
ϵ	Pore fraction at the mesoscale.
ν	Dynamic viscosity of the fluid, $m^2.s^{-1}$.
Ω	Fluid domain surrounding Σ, m^3.
ϕ_f	Volume fraction of fiber.
ϖ	Condensation ratio, $\varpi = \frac{c}{c_s}$.
Σ	Ablative surface, m^2.
τ_K	Transient evolution duration for $Da \ll 1$, s.

Latin symbols

c	Reactant concentration in Ω, $mol.m^{-3}$.
c_0	Reactant concentration in the nozzle core, $mol.m^{-3}$.

$\langle c \rangle$	Average reactant concentration, $mol.m^{-3}$.
$\tilde{c}$	Microscale reactant concentration deviation,$mol.m^{-3}$.
c_s	Solid concentration, $mol.m^{-3}$.
D	Reactant diffusion coefficient, $m^2.s^{-1}$.
Da_{eff}	Effective diffusivity for vertical diffusion, $m^2.s^{-1}$.
Da	Damköhler number, $Da = \frac{k\,l}{D}$.
$\langle Da \rangle$	Average Damköhler number, $\langle Da \rangle = \frac{\langle k \rangle l}{D}$.
E_a	Activation energy in k expression, $kcal.mol^{-1}$.
$\tilde{K}$	Ratio of reactivites between the solid phases.
k	Surface local reactivity, $m.s^{-1}$.
k_f	Fiber reactivity, $m.s^{-1}$.
k_m	Matrix reactivity, $m.s^{-1}$.
k_{eff}	Effective surface reactivity, $m.s^{-1}$.
$k^\star$	Harmonic average reactivity, $m.s^{-1}$.
$\langle k \rangle$	Superficial average reactivity, $m.s^{-1}$.
K_s	Pre-exponential coefficient, $m.s^{-1}.K^{-1}$.
l_μ	Microscale characteristic length, m.
l_m	Mesoscale characteristic length, m.
$\mathbf{n}$	Normal to Σ pointing towards the fluid, m.
Pe	Mass Péclet number, $Pe = \frac{u\,l}{D}$.
R_f	Fiber radius, m.
Re_μ	Microscale Reynolds number, $Re_\mu = \frac{u\,l_\mu}{\nu}$.
Re_m	Mesoscale Reynolds number, $Re_m = \frac{u\,l_m}{\nu}$.
Re_x	Position dependent Reynolds number, $Re_x = \frac{u\,x}{\nu}$.
$\mathbf{u}$	Fluid velocity in the local frame, $m.s^{-1}$.
$\boldsymbol{u}$	Fluid velocity in the global frame, $m.s^{-1}$.
$\mathbf{v}$	Local recession velocity in the global frame,$m.s^{-1}$.
$\mathbf{v}_a$	Average recession velocity in the global frame,$m.s^{-1}$.